

Cite this: *Mater. Adv.*, 2024,  
5, 6030

# Recent advancements in metal organic framework-modified multifunctional materials for photodynamic therapy

Archana Kumari Pattnaik,<sup>a</sup> Newmoon Priyadarshini,<sup>a</sup> Priyanka Priyadarshini,<sup>a</sup> Gobinda Chandra Behera<sup>b</sup> and Kulamani Parida<sup>ib</sup> \*<sup>a</sup>

Metal-organic frameworks (MOFs) are porous hybrid structures possessing great potential for application in therapeutic platforms, particularly phototherapy, owing to the vast number of functional moieties that can be employed in numerous synthetic procedures to achieve target-oriented structures. Presently, phototherapy is the most viable and emerging technology with daily advancements in photothermal (PT) agents to eradicate malignant diseases such as cancer. Over the last decade, nanoscale MOFs have vigorously bloomed as photodynamic (PD) agents owing to their porosity, biocompatibility, and photosensitizing ability and as nanocarriers. Besides, MOFs also exhibit synergistic effects of combined and image-guided therapies efficiently under both *in vitro* and *in vivo* conditions. In this review, we focus on the recent advancements in MOF-modified multifunctional agents for photodynamic therapy (PDT) and emphasize the light-triggering mechanism of PDT and its role in the destruction of targeted pathogens. Subsequently, we summarize various types of MOF-based photosensitizers in their parent and modified forms and their effect in enhancing therapeutic applications. Finally, we present the current challenges and future advancements in the application of MOFs in the wide arena of PDT.

Received 10th April 2024,  
Accepted 24th June 2024

DOI: 10.1039/d4ma00376d

rsc.li/materials-advances

## 1. Introduction

The effect of light on the treatment of diseases, including rickets, vitiligo, and skin cancer, dates back to more than 3000 years when the primeval civilization became aware of the benefits of light.<sup>1</sup> For the first time, the Nobel Prize was given to Niels Finsen in 1903 for curing cutaneous tuberculosis and smallpox pustules using UV and red light, which marked the beginning of “phototherapy”.<sup>1,2</sup> Subsequently, in 1975, Thomas Dougherty explored the use of light in the complete removal of tumor cells from mice for the first time.<sup>3</sup> In recent years, an increasing number of researchers have been exploring the use of phototherapy for treating both cancer and non-malignant diseases, leading to significant therapeutic achievements.<sup>4,5</sup> Hence, among the different available therapeutic methods, as demonstrated in Fig. 1, phototherapy is an emerging and the most highly promising therapeutic approach. PDT was discovered a century ago by Oscar Raab, who was working with Prof. Hermann von Tappeiner. Raab explored the degradation of paramecia when exposed to

light and a fluorescent dye;<sup>6</sup> Von Tappeiner introduced the term “photodynamic reaction”.<sup>7</sup>

Despite the many studies since the early 1900s, the clinical utility of PDT only started gaining widespread application after the 1970s.<sup>8</sup> Thus, PDT is considered a contemporary, non-invasive, and advanced technique to diagnose many illnesses. The spatiotemporal selectivity of PDT makes it a promising therapeutic option for a broad array of non-oncological and oncological disorders.<sup>9,10</sup> However, despite its broad and diverse therapeutic applications, the clinical use of PDT as a primary oncological treatment is still in its infancy. This is



Fig. 1 Various therapeutic approaches for cancer therapy.

<sup>a</sup> Centre for Nanoscience and Nanotechnology, Siksha 'O' Anusandhan (Deemed to be University), Bhubaneswar 751030, Odisha, India.

E-mail: kulamaniparida@soa.ac.in; Fax: +91-674-235064; Tel: +91-674-2351777

<sup>b</sup> Department of Chemistry, Maharaja Purna Chandra Autonomous College, Takhatpur, Baripada 757003, Odisha, India

primarily due to significant limitations, such as the absence of ideal photosensitizers (PS), difficulty in formulating PSs, selection of appropriate light dosimetry for effective treatment, and monitoring treatment responses; these challenges are the focal point of this review.<sup>11</sup> MOFs are promising porous (microporous/mesoporous) hybrid coordination-polymers composed of metal-ionic clusters as inorganic nodes and organic linkers as primary building blocks. Various types of MOFs have been extensively used in the fields of adsorption<sup>12</sup> and heterogeneous catalysis such as energy generation, organic transformations and pollutant degradation.<sup>13–16</sup> Besides, MOFs are highly useful for the fabrication of energy storage devices.<sup>17</sup> Additionally, they have been extensively employed in biomedical applications.<sup>18</sup> The unique crystalline structure of MOFs enables them to not only incorporate molecules in their pores but also allow the molecules of interest to coordinate with metals, assuming defined positions within their structure as building units. These characteristics lead to materials in which both the metals and molecules play crucial roles, offering numerous applications. In recent years, MOFs have been extensively employed in nanomedicine to enhance the efficacy and implement advanced strategies. Their tunable pore sizes make them promising drug carriers and the coordination bonds present in MOFs allow them to showcase targeted topologies, which are beneficial for stimuli-responsive drug release.<sup>19,20</sup> Additionally, nanoscale MOFs possess numerous reactive sites, which can be further modified, such as attaching targeting molecules, significantly enhancing the selectivity of nanoparticles (NPs) used in therapeutic applications. Through careful design, unique MOFs have been developed, which are biodegradable, nontoxic, possess minimal side effects and can be easily cleared from the body.<sup>21</sup> Consequently, the use of MOFs in phototherapeutic applications has been explored in the past decade and a rapidly increasing trend has observed in recent years, as shown in Fig. 2. MOFs can directly serve as PSs or photothermal agents (PTAs) with photo-responsive building units, thereby forming intrinsic photothermal or photodynamic MOFs.<sup>22–24</sup> Alternatively, they can exhibit photo-responsive capabilities by loading phototherapeutic agents<sup>24</sup> or the formation of core-shell structures and designing different composites.<sup>25</sup> Also, the modification of different MOFs can



Fig. 2 Number of publications on the use of MOF-based materials in PDT; result obtained from a Web of Science search conducted on 2nd June 2024.

be tailored to increase their light absorption range and electron transfer pathways by improving the efficacy of reactive oxygen species (ROS) generation. Furthermore, these modifications can help the particles better adapt to the physiological environment by alleviating hypoxia or attaching targeting molecules.<sup>20,26,27</sup> The application of MOF-based NPs in PDT also represents a significant advancement, addressing some of the limitations associated with traditional PS.<sup>28</sup>

In this critical review, initially, we introduce the principles of PDT and underlying principles of designing nanostructured MOFs as PSs and photo responsive agents in PDT. Particularly, we emphasize theranostic MOF agents and all their possible modifications for achieving benchmark activities in diagnosis using specific examples from recent publications. Finally, we offer an extensive overview of the current challenges and future perspectives of MOFs as PDT agents, highlighting their development at each stage. It is imperative to note that the articles cited in the current review do not detract from other pioneering contributions by numerous researchers in this field. To date, although there is significant growth in research on PDT for therapeutic applications and reports in the form of perspectives, comprehensive reviews, critical reviews, and mini reviews are available in the literature, there is still a need for a complete review focusing on the applications of MOF-based functionalized nanostructured materials in PDT, antimicrobial and antibacterial therapy, wound healing, and beyond.<sup>2,5,6,11,18,26,29</sup> Herein, we compile the relevant information concerning MOF-based photosensitizing agents for PDT applications. In this review, we elucidate the underlying mechanism of ROS generation, which is responsible for disrupting the phagocytic behavior of diseased cells. Besides, we highlight the unique properties of MOF-based PDT agents, such as their organic-inorganic porous structure, which enables the generation of ROS with minimal cytotoxicity. This review aims to inspire the development of newly designed hypotoxic MOF-based photosensitizers, thereby stimulating empirical research in various phototherapy treatments. Again, firstly, we outline the principles of PDT, followed by a comprehensive summary of the recent advances in MOFs for PDT, ranging from photo-responsive intrinsic MOFs to various functionalized MOFs. Subsequently, we classify numerous methods for the optimization of therapeutic systems. Our primary focus is discussing the function and contribution of MOFs in various therapeutic systems. Finally, we discuss the current challenges and drawbacks in this swiftly evolving research field.

## 2. Fundamental insights into PDT

### 2.1. Photodynamic reaction

PDT is a specialized form of phototherapy, which relies on the coordinated action of three key components, including a light source, a PS, and molecular oxygen. Firstly, a PS is injected into the patient's body through intravenous or topical applications, and consequently a critical phase known as the 'drug-light interval' ensues.<sup>5,9</sup> During this period, the PS accumulates





Scheme 1 Schematic representation of the PDT mechanism.

selectively in the targeted tissue, confirming that the desired concentration is achieved. Once the ideal distribution is achieved, light with a specific wavelength is directed at the targeted area, activating the PS.<sup>30,31</sup> The choice of wavelength is selected based on the distinctive absorption-spectrum of the employed PS, which is basically in the absorption spectrum range of 600 to 850 nm for PDT applications. This wavelength range defines the spectrum in which PS can efficiently absorb light. Each wavelength is comprised of the specific energy required to activate the PS, thereby facilitating energy transitions. The energy of absorbed light precisely matches the energy difference needed for an electron-transition between energy levels.<sup>32,33</sup> Upon illumination, the PS absorbs a photon and it undergoes a transition from the ground state (GS) to a short-lived singlet excited-state (ES) (1PS\*) (Scheme 1). Then, the excited PS (1PS\*) can return to the GS by emitting fluorescence, which can be utilized clinically for photodetection and imaging. Alternatively, it undergoes intersystem-crossing, where spin flipping of the excited electron results in the formation of a long-lasting triplet-ES (3PS\*).<sup>34</sup> Subsequently, the triplet-ES PS directly interacts with a substrate, such as a molecule and cell membrane transferring proton/electron to create anion/cation radicals. Subsequently, these free radicals react with molecular oxygen ( $O_2$ ) to generate ROS such as hydrogen peroxides ( $H_2O_2$ ), superoxide anion radical ( $O_2^{\bullet-}$ ), and hydroxyl radicals ( $HO^{\bullet}$ ) (type-I reaction). Then, energy transfer directly occurs from the excited PS to  $O_2$ , leading to the formation of singlet-oxygen ( $^1O_2$ , a type II reaction). Actually, 22 kcal mol<sup>-1</sup> (corresponds to a wavelength of 1274 nm) energy is required for  $O_2$  to transition from its ground triplet-state to the singlet excited-state.<sup>35</sup> Hence, a small amount of energy is required to generate  $^1O_2$ .<sup>36</sup>

In PDT, the by-products obtained from type-II and type-I reactions are the agents responsible for therapeutic effects and cell-killing. Also, it is imperative to note that both reactions (type-I and type-II) occur concurrently. However, most reported studies specify the prevalence of type-II reactions, highlighting the dominant role of  $^1O_2$  in PDT.<sup>30,31,37</sup>

## 2.2. Tumor demolition mechanism

After PDT, the rate of photo-induced tumor killing is influenced by several factors, including the nature, concentration, and position of the PS within the tumor or sub-cellular location during light irradiation. Other factors include the duration between light irradiation and PS administration, which is popularly known as the drug-light-interval, *i.e.* DLI, light influence rate, rate of total influence, specific tumor type, and tumor oxygenation level.<sup>38,39</sup> The downstream targets of PDT involve the tumor microvasculature, normal microvasculature, tumor cells, and inflammatory immune-host system. The photo-produced ROS during the PDT reaction are the called primary effectors, enabling permanent damage to the microvasculature and tumor cells. This procedure activates several of immune and inflammatory responses, which in combination contribute to achieving long-term tumor cell control.<sup>36,40</sup>

As discussed earlier in Section 2.1, both type-I and type-II reactions of PDT occur concurrently and contribute to therapeutic effects, thereby inducing cell death.<sup>5,41</sup> Various factors are responsible for balancing these reactions including the substrate/target tissue, inherent feature of the PS, binding affinity of the PS to the substrate and concentration of local oxygen.<sup>35</sup> In both type-I and type-II reactions, initially the PS is in a singlet excited-state due to the transfer of photon energy from light illumination. Then, it undergoes intersystem crossing for a transition to a long-lived, more stable, and electronically triplet ES.<sup>35</sup> In the type-I reaction, the triplet ES of the PS interacts directly with the substrate, which can be a cell membrane or other molecule. This type of biochemical interaction enables cell-damage through two basic primary processes of electron transfer reactions or hydrogen-atom abstraction (Scheme 2). Consequently, extremely reactive radical ions and free radicals are generated from the reactions with cellular components such as proteins and lipids from the lipid membrane, leading to instant cell-damage. Moreover, these free radicals can react with  $O_2$  to produce various ROS ( $O_2^{\bullet-}$ ,  $HO^{\bullet}$ , and  $H_2O_2$ ), which cause oxidative damage to biological structures, ultimately leading to cell death.<sup>3,5,20,42,43</sup>





**Scheme 2** Mechanism of PDT in tumor destruction using PSs and photo-produced ROS after light irradiation. Adapted with permission from ref. 43 Copyright Elsevier, 2021.

### 3. Photosensitizer

An ideal photosensitizer is expected to exhibit preferential accumulation in tumour tissues, while instantly clearing from normal tissues. Amphiphilicity is another crucial parameter for a clinically effective PS, given that it should be able to travel to the targeted tumor tissue unimpeded when administered systemically, requiring a degree-of-hydrophilicity, and attach to the target cells, necessitating a degree-of-lipophilicity. Additionally, it should have minimal dark-toxicity, an elevated quantum yield of triplet ES formation, and suitable lifetime of triplet-state to interact with GS oxygen or other substrates for the generation of surplus ROS. Basically, the PS should be induced/activated by light of higher wavelengths ( $> 700$  nm) for deeper penetration into tissues because the strong light absorption of haemoglobin below 700 nm inhibits deep penetration in target tissues.<sup>11,34</sup> Presently, despite the fact that they do not satisfy all the required criteria, several PSs have been approved for clinical applications due to their enhanced efficacy execution in antitumor treatment and some are undergoing clinical trials. These PSs predominantly belong to the category of first- and second-generation PSs.

Generally, first-generation-PSs are porphyrin-based materials explored between the 1970s–1980s. For example, hematoporphyrin-derivatives (HpD) that contain an exclusive mixture of porphyrin monomers, oligomers, dimers, and porfimer sodium (active material in HpD).<sup>42,44</sup> Porfimer sodium offers numerous advantages such as tumor destruction, easy formulation of water-soluble intravenous delivery and minimal dark toxicity. However, its narrow light absorption range in the red part of the solar spectrum (optimal for tissue-penetration) often necessitates the administration of large amounts of drug to achieve a benchmark phototherapeutic response.<sup>45</sup>

Second-generation-PSs, known as porphyrinoid-based compounds, consist of porphyrin/porphyrin-modified macrocyclic

rings, such as chlorins, phthalocyanines, bacteriochlorins, bacteriopheophorbies, pheophorbides, texaphyrins, and non-porphyrinoid compounds such as phenothiazines, anthraquinones, cyanines, curcuminoids, and xanthenes.<sup>46</sup> They also include metalated derivatives of PSs, *e.g.* tin ethyl etiopurpurin ( $\text{SnET}_2$ ), Si(IV)-naphthalocyanine (SiNC), and aluminum phthalocyanine tetrasulfonate ( $\text{AlPcS}_4$ ).<sup>47</sup> These PSs were developed in the late 1980s to address the issues of first-generation PSs owing to their high extinction coefficients and broad absorption maxima at longer wavelengths than 630 nm. In general, these PSs exhibit higher  $^1\text{O}_2$  quantum yields and a higher concentration in tumor tissue compared to HpD, enabling an effective antitumor effect. Moreover, the treatment time can be reduced owing to their much shorter tissue accumulation time, and most importantly the PDT procedure can be implemented on the same day of drug administration. Accordingly, PDT can be an acceptable outpatient procedure for patients. Furthermore, these PSs exhibit a shorter window, *i.e.* less than two weeks, of cutaneous photosensitivity.<sup>48,49</sup>

Third-generation-PSs are activated with longer wavelength light, enabling minimal photo-sensitivity and improved tumor-specificity.<sup>50</sup> This can be achieved as follows: (a) chemically conjugating or encapsulating PSs in carriers/delivery-vehicles, which can transport drugs efficiently in the bloodstream from the drug-administration site to the targeted tissue and (b) modifying the pristine PSs with biological conjugates (antibodies, peptides, and antisense molecules) for achieving tumor-specific targeting of PSs.<sup>51</sup> In essence, these PSs represent an enhancement in second-generation-PSs in terms of targeting capabilities or delivery. However, although many 3rd-generation-PSs have been extensively studied and accountable for selective *in vitro* targeting, much less PSs have been evaluated for clinical applications due to their insufficient *in vivo* selectivity.<sup>52,53</sup> The various types of PSs used in PDT are presented in Scheme 3.





Scheme 3 Photosensitizers used in PDT. Adapted with permission from ref. 20 RSC 2021.

## 4. Application of MOFs in PDT

The utility of MOFs in PDT has been well explored in recent times because of their intriguing structural features and wide range of functional moieties, delivering various physico-chemical characteristics such as porosity, biocompatibility, presence of active sites, storage capacity, and feasibility. Some of these photodynamic agents are discussed below and their characteristic features together with their reference are presented in detail in Table 1.

### 4.1. Intrinsic photodynamic MOFs

**4.1.1. Porphyrin-based intrinsic MOFs.** Porphyrins and their variations have been widely employed in PDT as photosensitizers. Utilizing porphyrins and their variations directly as organic ligands is a prevalent approach in the preparation of inherent photodynamic MOFs.

The orderly arrangement of porphyrin molecules within the framework of MOFs enhances their hydrophobicity, inhibits self-aggregation, and boosts the production of  $^1\text{O}_2$ . Additionally, the MOF structure promotes the efficient drug loading of porphyrin molecules, facilitates the entry of oxygen, and aids the diffusion of  $^1\text{O}_2$ , thereby preventing self-quenching. Numerous studies have successfully synthesized MOFs incorporating porphyrins, which were designed for PDT and combined therapeutic approaches.

Importantly, these macrocyclic conjugated structures produce visible light absorption bands and when irradiated,

generate fluorescence, making them useful for imaging of the infected region and leading to diagnosis by analysis of the obtained spectrum. In this regard, Tian and coworkers designed a core-satellite porphyrin-based MOF by integrating it with CuS (HP-PCN@CuS). HP-PCN@CuS possessed a hierarchically porous structure, where the highly oxygen-efficient PCN-224 is an intrinsic nano-PS, and thus it delivered a photodynamic therapeutic effect with easy ROS generation.<sup>22</sup> However, its antitumor effect was restricted by the poor laser penetration and hypotoxic tumor environment. Thus, to overcome this issue, CuS NPs were implemented owing to their excellent antitumor efficacy, promising anti-tumour property, nanosize for easy removal and deep penetration in tumor cells with low toxicity to normal cells. Again, *in vivo* and *in vitro* studies demonstrated their combined CDT/PTT/PDT effect to inhibit tumor growth with low cytotoxicity, as shown in Fig. 3(a).

In another study, Zhao *et al.* prepared a gold nanocluster-modified Zr-MOF with PCN-224 nanozyme with enzyme mimetic activities, which was found to be an excellent probe for ROS generation under NIR laser light irradiation.<sup>55</sup> This biomaterial of AuNCs@PCN loaded in hydrogel is an excellent cell repair material, which is useful in diabetic infected wound healing and modification with Au NC contributes to extreme stability and biocompatibility. The antibacterial performance of the material was also evaluated *in vitro* using MRSA and Amp<sup>r</sup> *E. coli* as representative bacteria. The Au NCs exhibited Fenton-like activity responsible for ROS generation in the wound site for CDT and PDT. Also, the ROS within the bacteria were



Table 1 Summary of recent MOF-based PDT agents used as imaging theranostic platforms

| MOF-based therapeutic agents | Precursors  | Particle size (nm) | Light source ( $\lambda$ , nm) | <i>In vitro</i> cell lines   | <i>In vivo</i> models                                      | Imaging method and biomedical application  | Type of delivery | Ref. |
|------------------------------|---|--------------------|--------------------------------|--|--|--|------------------|------|
| HP-PCN@CuS                   | H <sub>2</sub> TCPP<br>ZrOCl <sub>2</sub> ·8H <sub>2</sub> O<br>CuS   | 236.8 ± 8.1        | 660                            | 4T1, HepG2, Caco-2 and L02 cells   | 4T1 tumor bearing mice                                     | PT imaging and anti-cancer therapy   | Intravenous      | 54   |
| Au NCs@PCN@H                 | PCN-224<br>HAuCl <sub>4</sub><br>NaBH <sub>4</sub><br>PVA<br>Alg  | 190                | 380                            | <i>S. aureus</i><br>MRSA<br><i>E. coli</i><br>Amp <sup>r</sup><br><i>E. coli</i> | HUVECs<br>HACATs   | Thermal imaging and diabetic wound healing   | Intraperitoneal  | 55   |
| siRNA/Zr-FeP                 | H <sub>4</sub> TBP-Fe<br>Zr <sub>6</sub> clusters<br>Heat shock protein 70 siRNA  | 210                | 635                            | MCF-7 cells  | MCF-7 cells injected to underarm of female mouse           | IR/CT imaging and anti-cancer therapy  | Intravenous      | 56   |
| PCN-DOX@PDA                  | PCN-600<br>Polydopamine (PDA)<br>Doxorubicin (DOX)  | 180                | 633                            | 4T1 cells  | 4T1 tumor-bearing mice model                               | MR imaging and Tumor Theranostics  | Intratumoral     | 57   |
| Ti-TBP                       | TiCl <sub>4</sub> ·2THF<br>H <sub>4</sub> TBP   | 100.1 ± 4.0        | 650                            | CT26 cells   | CT26 tumor-bearing BALB/c mice model                       | Confocal imaging and antitumor therapy   | Intratumoral     | 58   |
| HUC-PEG                      | Hf-UiO-AM TAPC<br>Terephthaldehyde<br>PEG5k-NH <sub>2</sub>   | 179                | 671                            | HeLa cells   | Cervical cancer cells of mouse (U14)                       | CT/PT imaging and tumor cell treatment   | Intravenous      | 59   |
| CuTz-1-O <sub>2</sub> @F127  | {Cu <sub>3</sub> [Cu <sub>5</sub> (3,5-Ph <sub>2</sub> -tz) <sub>6</sub> ] <sub>n</sub> } <sup>2+</sup><br>F127                         | 100                | 808                            | HeLa cells<br>L929 cells<br>4T1 cells  | 4T1 tumor bearing Balb/c mice                              | Removal of hypoxia microenvironment, antitumor therapy                                       | Intravenous      | 60   |
| DNAzyme/[Cu(tz)]             | Cu(NO <sub>3</sub> ) <sub>2</sub> ·3H <sub>2</sub> O<br>Htz<br>Cu <sub>2</sub> O nanoparticles<br>DNAzyme (Cy5-DNAzyme and Ce6-DNAzyme) | 500                | 660<br>808                     | MCF-7 cells  | MCF-7 tumor bearing female Balb/c mice                     | Confocal imaging and gene silence therapy, hypoxia removal and anti-tumor therapy            | Intravenous      | 61   |
| UiO-PDT                      | UiO-66<br>BODIPYs (I2-BDP)  | 70                 | 525                            | B16F10   |  | Anti-cancer therapy  |                  | 62   |
| UiO-66 modified              | UiO-66<br>TCPP<br>BCDTE   | 70                 | 420                            | B16  |  | Control PDT  |                  | 63   |
| Ce6@MOF-Gel                  | Zn <sup>2+</sup><br>FMOC-His<br>Ce6<br>F127<br>Alginate   |                    | 660                            | Mouse fibroblasts L929<br>Mouse embryo fibroblasts 3T3                           | <i>S. aureus</i>   | Wound healing and antibacterial therapy  | Topical          | 64   |
| UCZRF                        | UCNPs ( $\beta$ -NaYF <sub>4</sub> :20%Yb, 2%Er)<br>ZIF-8<br>Cu(NO <sub>3</sub> ) <sub>2</sub> ·3H <sub>2</sub> O<br>Rose Bengal        | 40                 | 980                            | 4T1 cells in BALB/c mice   | 4T1 cells in BALB/c mice                                   | Antitumor effect   | Intravenous      | 65   |
| HDPI                         | HKUST-1<br>DMSNs-Pt(IV)<br>ICG  | 281                | 808                            | 4T1 cells  | H22 cancer bearing Balb/c mice                             | NIR/MR imaging   | Intravenous      | 66   |
| Cu-MOF@RCD                   | Cu(OAc) <sub>2</sub><br>H <sub>3</sub> BTC<br>Red Carbon Dots   | 30 ± 3             | 650                            |  | Bilateral CT26 tumor bearing 7 week old female Balb/c mice | PT imaging and Checkpoint blockade immunotherapy with anti-PD-L1, multi-modal cancer therapy | Intraperitoneal  | 67   |



Table 1 (continued)

| MOF-based therapeutic agents      | Precursors   | Particle size (nm)             | Light source ( $\lambda$ , nm) | <i>In vitro</i> cell lines             | <i>In vivo</i> models                   | Imaging method and biomedical application                              | Type of delivery             | Ref. |
|-----------------------------------|--|--------------------------------|--------------------------------|--|---|--|------------------------------|------|
| PS@MOF-199                        | MOF-199<br>PS $\approx$ Ce6, TPAAQ<br>F127   | 150                            | 400–700                        | HepG2 cells<br>NIH-3T3                 | 4T1 tumor bearing mice                  | Confocal imaging and antitumor therapy                                 | Intratumoral/<br>intravenous | 68   |
| F127-TPETCF@MIL-100               | MIL-100 (Fe)<br>TPETCF<br>F127   | 140                            | 400–700                        | 4T1 cells                              | 4T1 tumor-bearing mice model            | CLSM imaging and antitumor therapy                                     | Intravenous                  | 69   |
| ZIF-8/DA-0.5/ICG                  | ZIF-8<br>DOPAMINE (DA)<br>ICG  | 295                            | 808                            | <i>S. aureus</i> and<br><i>E. coli</i> |   | IR thermal imaging and antibacterial Therapy                           | Intravenous                  | 70   |
| Pt-carbon nanozyme                | ZIF-8 SiO <sub>2</sub> NaBH <sub>4</sub> H <sub>2</sub> PtCl <sub>5</sub>  | 122                            | 808                            | CT26 sub-cutaneous tumor model         | CT26 sub-cutaneous tumor model          | PT imaging and tumor cell/removal of tumor hypoxia in microenvironment | Intravenous                  | 71   |
| NT@PEG@FA                         | NU-1000<br>TCPP<br>PEG<br>FA   | 100                            | 650                            | HeLa cells                             | HeLa cells                              | Fluorescence imaging and anti-tumor PDT                                | Intravenous                  | 72   |
| UCNR@MIL-100(Fe)                  | MIL-100(Fe)<br>b-Phase NaYF <sub>4</sub> :Yb,Tm,Gd   |                                | 980                            | <i>S. aureus</i> and<br><i>E. coli</i> |   | Antibacterial therapy  |                              | 73   |
| UCTSCF                            | IL-100(Cu/Fe)<br>chlorin e6 (Ce6)<br>TFS@mSiO <sub>2</sub>   |                                | 808                            | L929 or MCF-7 cells                    |   | CLSM imaging and antitumor therapy                                     |                              | 74   |
| Au@MOF-FA                         | [Fe <sub>3</sub> O(OAc) <sub>6</sub> (H <sub>2</sub> O) <sub>3</sub> ]NO <sub>3</sub> ·2H <sub>2</sub> O<br>Au NRs<br>Folic acid |                                | 660                            | CaSki cells                            | CaSki tumor-bearing mouse model         | CLSM imaging and antitumor therapy                                     | Intratumoral                 | 75   |
| Zr-MOF@PPa/AF                     | ZrCl <sub>4</sub><br>2-Amino terephthalic acid<br>Pyrophephorbide-a (PPa)<br>6-Amino flavone (AF)                                | 87                             | 671                            | HepG-2<br>4 T1                         | 4 T1-bearing male Balb/c mice           | Fluorescence imaging<br>PDT-CT   | Intratumoral                 | 76   |
| LSSPL                             | Erythromycin-loaded liposomes<br>Pullulanpheophorbide A (PU-Pheo A)<br>DPPC<br>Cholesterol                                       | 93.63 $\pm$ 3.1 (hydrodynamic) | 675                            | <i>P. acne</i>                         | <i>P. acne</i> in male BALB/c nude mice | Antimicrobial treatment  | Intradermal                  | 77   |
| DOX/poly(DH-Se)/PEG/PPG urethane) | PCN 224<br>DOX<br>Di-(1-hydroxylundecyl)selenide (DH-Se)<br>PEG, PPG   | 225 $\pm$ 58                   | 488                            | HepG2                                  | HepG2 liver cancer cells in nude mice   | Fluorescence imaging<br>PDT-CT   | Intravenous                  | 78   |
| SR@PMOF                           | Zr cluster<br>TCPP<br>SR-717   | 50                             | 650                            |  | 4T1 cells in Female Balb/c mice         | PDT-STING immunotherapy  | Intravenous                  | 79   |

detected by the fluorescent probe DCFH-DA. The detailed underlying mechanism for the antibacterial degradation is depicted in Fig. 3(b) and (c).

It is worth noting that mixed-metal MOFs with photosensitive ligands as linkers have attracted immense attention owing to their intriguing features compared to conventional MOFs. To achieve this, Zhang *et al.* designed a Zr-ferriporphyrin MOF, which readily facilitated ROS generation and multimodal

imaging, and thus responsible for the theranostic<sup>56</sup> effect in cancer therapy. Zr-FeP was modified by siRNA and PEG and formed a nano-shuttle, which is a drug vehicle with multifunctional effects such as easy release under acidic conditions, good stability, biocompatibility and low cytotoxicity for biomedical applications.<sup>56</sup> This ideal PS when irradiated in the NIR region generated both  $\bullet$ OH and  $^1$ O<sub>2</sub>. Besides, Zr-FeP MOF also facilitated synergistic applications such as low-temperature PTT



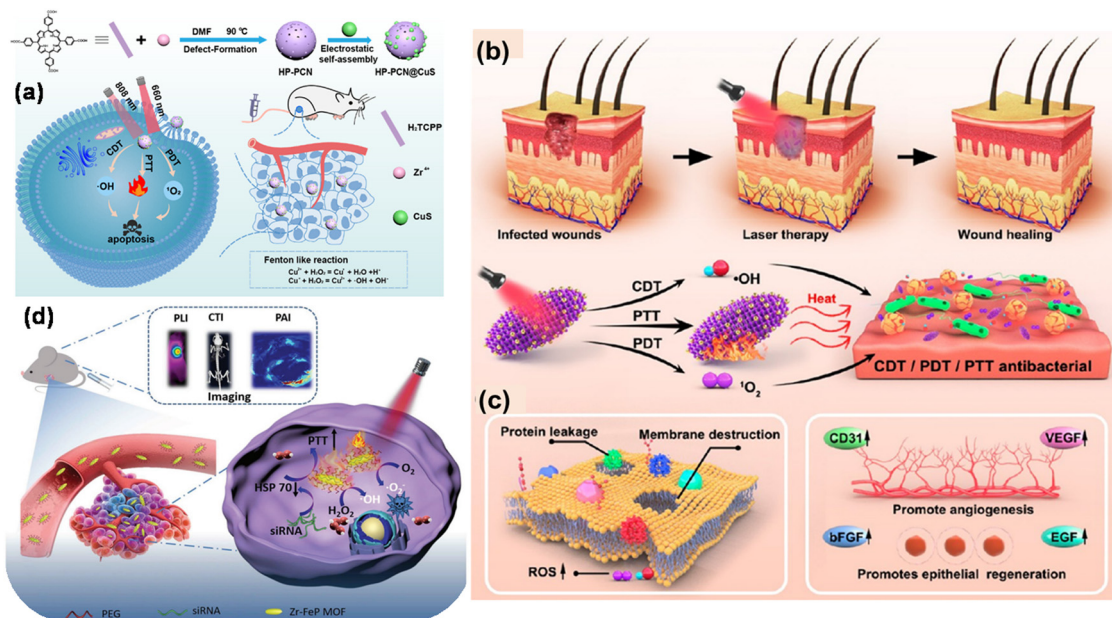


Fig. 3 (a) Scheme showing the fabrication and mechanism of combined cancer therapy using HP-PCN@CuS. Adapted with permission from ref. 22 Copyright Elsevier, 2022. (b) and (c) High-temperature destruction of MDR pathogens using PDT/CDT/PTT using Au NCs@PCN and disruption of protein leakage and bacterial membrane structure for promoting epithelial cell repair and angiogenesis through the up-regulation of the expression of many related factors. Adapted with permission from ref. 55 Copyright ACS, 2022. (d) Schematic showing multimode imaging diagnosis using siRNA/Zr-FeP MOF nano-shuttle and combined PTT/PDT for cancer treatment. Adapted with permission from ref. 56 Copyright Wiley, 2018.

and silencing Hsp70. The multimode imaging diagnosis using siRNA/Zr-FeP MOF for cancer treatment is depicted in Fig. 3(d). The *in vitro* anti-cancer efficacy of cell death ratio was 87.5%, showing the good therapeutic use of the fabricated nano-shuttle.

Chen *et al.* developed an NIR and pH-responsive system (PCN-DOX@PDA) for tumor diagnosis and treatment, combining MRI-enabled chemotherapy with photothermal and photodynamic therapy (Fig. 4a).<sup>57</sup> This system contained PCN-600, a

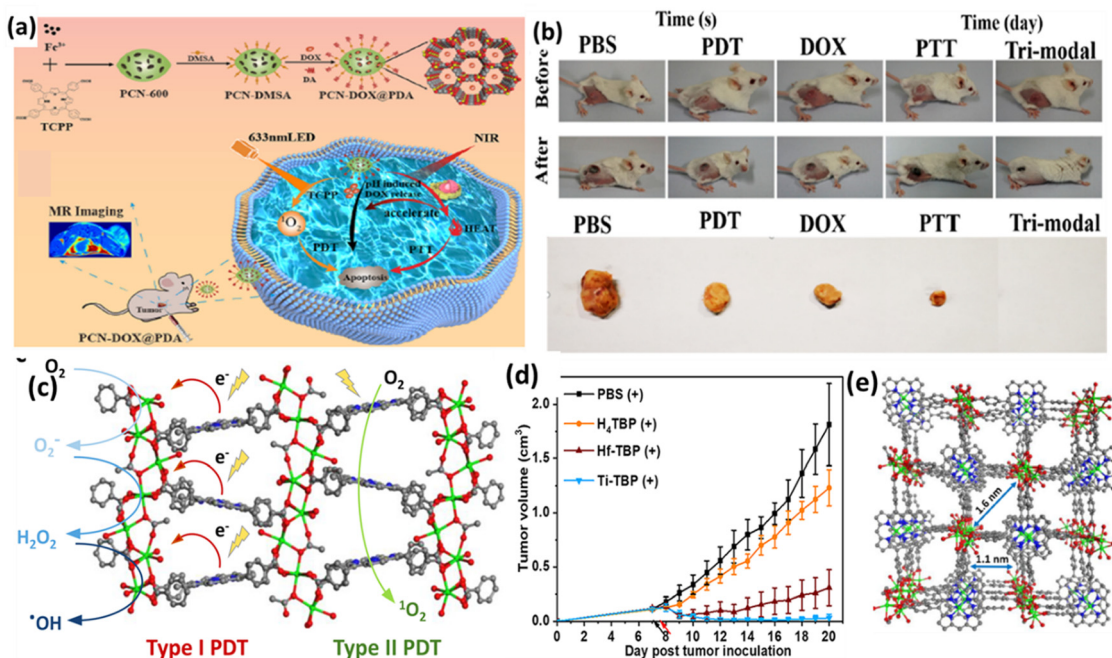


Fig. 4 (a) and (b) Scheme illustrating the design of PCN-DOX@PDA with lethal mechanism model against tumor cells and digital photographs of 4T1 tumor-bearing mice. Adapted with permission from ref. 57 Copyright ACS, 2023. (c) Type-I and Type-II PDT mechanism, (d) *in vivo* anti-cancer outcome on CT26 tumor-bearing mice, and (e) perspectives of structure of Ti-(Ti-TBP). Reprinted with permission from ref. 58 Copyright RSC, 2024.



porous MOF, as a carrier for antitumor drugs and polydopamine, with its photosensitive ligand TCPP generating  $^1\text{O}_2$  under NIR irradiation. The weak acidic tumor environment triggered the degradation of PCN-DOX@PDA, releasing the drugs in a controlled manner, which was enhanced by the heating effect of photothermal therapy. The PCN@PDA nanoparticles exhibited high photothermal efficiency and stability, heating consistently under 808 nm laser and generating singlet oxygen for photodynamic therapy, as shown by the decrease in absorbance at 417 nm. Encapsulating doxorubicin (DOX) in PCN@PDA increased the drug loading, enhancing its promise for photothermal therapy and photodynamic treatment. The PCN-DOX@PDA nanoparticles (NPs) effectively generated reactive oxygen species (ROS) and exhibited remarkable antitumor effects under dual 808 nm and 633 nm light irradiation, leading to a significant increase in apoptotic or dead 4T1 cells, with a 59.1% apoptosis rate. The *in vivo* experiments on 4T1 tumor-bearing mice showed that although PCN@PDA NPs with individual light irradiation had limited tumor growth inhibition, the combination of PCN-DOX@PDA NPs with dual light irradiation resulted in almost complete tumor ablation without relapse, demonstrating superior antitumor efficacy (Fig. 4b). Furthermore, H&E staining confirmed the good biocompatibility of the NPs. These results suggest that PCN-DOX@PDA NPs are a promising and efficient tumor treatment strategy with excellent biocompatibility and therapeutic potential.

A novel nanoscale MOF (nMOF) called Ti-TBP was developed for PDT by Lin and team to enhance the efficacy in hypoxic

solid tumors.<sup>58</sup> Ti-TBP was comprised of Ti-oxo chains as secondary building units (SBUs) and photosensitizing ligands (5,10,15,20-tetra(*p*-benzoato)porphyrin (TBP)), enabling a hypoxia-tolerant type-I mechanism unlike traditional oxygen-dependent type-II PDT (Fig. 4c). Upon light irradiation, Ti-TBP generates singlet oxygen and facilitates electron transfer from the excited TBP\* moiety to the  $\text{Ti}^{4+}$ -based SBUs, resulting in the formation of  $\text{TBP}^{\bullet+}$  ligands and  $\text{Ti}^{3+}$  centers. This process produces multiple ROSS, as demonstrated by luminescence quenching, EPR spectra, and scavenging tests. The *in vivo* studies on a CT26 tumor-bearing BALB/c mouse model showed that Ti-TBP treatment led to significant tumor regression, with a 98.4% reduction in tumor volume and 60% cure rate, outperforming the Hf-TBP and  $\text{H}_4\text{TBP}$  treatments (Fig. 4d). The histological analyses indicated severe necrosis in the tumor slices from Ti-TBP treatment, while the steady body weights and lack of abnormalities in the major organ slices suggested the absence of systemic toxicity. The proximity of the Ti-oxo chain SBUs to TBP ligands in Ti-TBP structure, as shown in Fig. 4(e), facilitates electron transfer, making it a promising strategy for effective cancer treatment with nMOFs.

**4.1.2. Other photodynamic building blocks.** Porphyrin-adapted porous-organic-polymeric structures are promising candidates towards theranostics. However, their uncontrollable particle-size and uncertain mechanisms of photoactive reaction make them the “Achilles’ heels” for the therapeutic application. In terms of photodynamic building blocks besides porphyrins, Zheng *et al.* reported the fabrication of an integrated



Fig. 5 (a) *In vitro* and *in vivo* CT/imaging-guided photothermal therapy for HUC-PEG, (b) interface-enhanced phototherapy mechanism, and (c) tumour photographs with average weight variations in the mice in five groups. Adapted with permission from ref. 59 Copyright Elsevier, 2020.



nanocomposite MOF@POP-PEG named HUC-PEG by introducing TAPC (tetrakis(4-aminophenyl)-21*H*,23*H*-chlorin), PEG5k-NH<sub>2</sub> and terephthalaldehyde on the outer surface of the amine-functional Hf-UiO-66 MOF (Hf-UiO-AM) for “proof of principle”.<sup>59</sup> The PEG coating ensured that HUC-PEG remained well-dispersed and stable in the bloodstream, enhancing the drug accumulation within tumors. The incorporation of chlorin-based components improved the photon utilization efficiency, extending the treatment depth and enhancing the *in vivo* effectiveness. In both laboratory and animal studies, the HUC-PEG nanocomposite, comprised of non-photoactive Hf-UiO-AM MOF (0) and photoactive POPs (1), demonstrated an amplification effect (“0 + 1 > 1”), resulting in simultaneous improvements in the PDT and PTT performance, as shown in Fig. 5(a). The interface effect between two porous substances plays a major role in the enhancing <sup>1</sup>O<sub>2</sub> generation for PDT. Thus, the combination of non-photoactive MOFs such as Hf-UiO-AM (0) and photoactive POPs (1) 0 + 1 > 1 to form a nanocomposite enhances the PDT/PTT effect with controllable photo-properties. The Zr MOF core containing Hf element with strong X-ray attenuating and photothermal conversion ability played a role in the CT/PT imaging functions, whereas POP or COF synthesized from the organic building blocks TAPC and terephthalaldehyde facilitated ROS generation. The spatial arrangement of integrated structure together with macrocyclic conjugated tetratopic chlorin fragment and bimetallic cluster

enhances the ROS generation due to the interface effect, which was not effective in either case independently. The potential photoactive mechanism is illustrated in Fig. 5(b).

In addition to serving as a self-template for the formation of the MOF-POP hybrid and introducing imaging capabilities in the Hf-UiO-AM core, the indirect interactions between Hf and TAPC within the interface could increase the intersystem crossing of activated TAPC through the “heavy atom effect” or by forming heterogeneous junctions. These interactions result in more efficient energy transfer from the T1 state to the surrounding <sup>1</sup>O<sub>2</sub> for PDT and non-radiative transition from T1 to S0 for PTT compared to its Zr-based counterpart. After successful tumor suppression *in vitro*, this method was also implemented *in vivo* in U14 cells. Biocompatible HUC-PEG was administrated intravenously followed by 671 nm light irradiation after 12 h of drug administration, resulting in 69.7% tumor cell suppression with an increase in antitumor activity on the target area in the theranostic platform. The noticeable changes in tumor weights, as shown in Fig. 5(c), proved the outstanding antitumor activity of HUC-PEG.

In another study, Cai *et al.* synthesized CuTz-1 MOF, which was comprised of 3,5-diphenyl-1,2,4-triazole as a linker and Cu(I) as inorganic nodes and loaded with O<sub>2</sub>.<sup>60</sup> To enhance its biocompatibility, F127 was applied as a coating on CuTz-1. The mixed-valence structure of Cu(I) and Cu(II) in the MOF induced



Fig. 6 (a) Mechanism of PDT in CuTz-1-O<sub>2</sub>@F127, (b) *in vitro* PDT effect of CuTz-1@F127 and CuTz-1-O<sub>2</sub>@F127 against 4T1 cells under laser irradiation (808 nm) in hypoxic or normoxic conditions and (c) *in vivo* antitumor efficacy of CuTz-1-based nanoplatform on 4T1 tumor-bearing Balb/c mice. Adapted with permission from ref. 59 Copyright Wiley, 2019.



an intervalence charge-transfer mechanism and d–d transition, leading to absorption in the visible and NIR regions.

Upon exposure to 808 nm NIR light, the MOF underwent type-I PDT, generating  $\cdot\text{OH}$  and  $\cdot\text{O}_2^-$  through a Fenton-like reaction. Additionally, Cu(I) could interact with GSH, reducing the loss of ROS. The loaded  $\text{O}_2$  also helped alleviate hypoxia in the tumor environment. Furthermore, the CuTz-1 MOF could function as a light-triggered PS, producing  $\cdot\text{OH}$  and  $\cdot\text{O}_2^-$  in the presence  $\text{H}_2\text{O}_2$ , a process known as type-I PDT, as illustrated in Fig. 6(a). Again, both normoxic and hypoxic conditions were measured upon incubating CuTz-1@F127 and CuTz-1- $\text{O}_2$ @F127 with 4T1 cells under light illumination for 24 h (Fig. 6b). Additionally, CuTz-1@F127 could transport  $\text{O}_2$  molecules into cancer cells and absorb intracellular GSH, thus mitigating both hypoxia and GSH overexpression simultaneously. This capability significantly enhanced the effectiveness of PDT. Under light irradiation, CuTz-1- $\text{O}_2$ @F127 expressed better suppression activity compared to CuTz-1@F127 due to its greater content of  $\text{O}_2$  (Fig. 6c).

Liu *et al.* reported the synthesis of an ultrathin nano-2D sheet of copper coordination polymer with a thickness of  $4.5 \pm 0.8$  nm as an effective DNAzyme nano-carrier for intrinsic photosensitizer and gene therapy for removing hypoxia, thus enhancing PDT and facilitating Fenton-like reactions.<sup>61</sup> Planar [Cu(tz)] layer stacking with an interlayer distance of 0.31 nm was reported from three coordinated 1,2,4-triazolate (tz) ligands with a Cu(I) metal centre, as shown in Fig. 7(a) inset. The gene silencing technique was used to target cancer cells of early growth response factor-1 (EGR-1) with messenger RNA to diminish the expression of abnormal genes. In this process, the nano-carrier, chlorin e6, encapsulated by CP nanosheets played a vital role given that it targeted the cell efficiently without degradation, followed by deep penetration and

endosomal escape. The main advantage of these multifunctional nano-carriers is that they exhibit both type-I and type-II PDT in combination with gene silencing, providing an efficient therapeutic platform for cancer treatment. Type-II PDT is oxygen dependent, which produces  $^1\text{O}_2$  from molecular oxygen, thus creating hypoxia in TME, whereas type-I PDT is hypoxia tolerant, and both effects are possible due to the disassembly of DNAzyme/[Cu(tz)] in response to the GSH level at TME, facilitating Fenton-like reaction. The Cu(tz) nanosheets, as intrinsic PS, together with the redox chemistry of Cu(I)/Cu(II) enabled ROS( $\text{OH}\cdot$ ) generation in the presence of  $\text{H}_2\text{O}_2$ . The proposed combination therapy mechanism is presented in detail in Fig. 7(a). This study highlights the use of nonporous low-dimensional CPs as a new horizon for phototherapy, gene delivery and other biomedical applications.

In a separate investigation, Wang and colleagues devised a Zr-based nanoscale MOF called UiO-PDT by incorporating BODIPY *via* the ligand exchange solvent-assisted method.<sup>62</sup> UiO-PDT demonstrated outstanding biocompatibility and highly effective generation of ROS, leading to the efficient eradication of cancer cells. The *in vitro* phototoxicity of UiO-PDT was assessed using the MTT assay against the B16F10, CT26, and C26 cell lines under irradiation, as shown in Fig. 7(b), where free I2-BDP possessed low dark cytotoxicity and high phototoxicity for all the tested cell lines. Park and colleagues incorporated TCPP and 1,2-bis(5-(4-carboxyphenyl)-2-methylthien-3-yl) cyclopent-1-ene (BCDTE) in UiO-66 *in situ* to create a photochromic switch for generating  $^1\text{O}_2$ . The photoisomerization of BCDTE could transition TCPP from a state where it quenches  $^1\text{O}_2$  to an activated state. Under UV light irradiation, BCDTE existed in two isomeric forms (open and closed form), which had different absorption spectra. In the open form, TCPP in the triplet state ( $T_1$ ) could react with oxygen



Fig. 7 (a) Proposed combination therapy of DNAzyme-based gene silencing. Adapted with permission from ref. 60 Copyright Wiley, 2021. (b) *In vitro* cytotoxicities of free I2-BDP and UiO-PDT nanocrystals against B16F10 cells before and after light irradiation. Adapted with permission from ref. 61 Copyright RSC, 2016. (c) Proposed scheme of  $^1\text{O}_2$  control via competitive energy-transfer paths upon photoisomerization. Adapted with permission from ref. 62 Copyright Wiley, 2016.



to produce  $^1\text{O}_2$ . Conversely, when BCDTE was in the closed form, it had an alternative energy transfer pathway with TCPP, which could impede the reaction between TCPP and oxygen, thereby quenching the generation of  $^1\text{O}_2$ , as represented in Fig. 7(c).<sup>63</sup> This work is considered an effective strategy with the cell model serving as a protective formula in PS delivery.

#### 4.2. Modifications with photodynamic agents

Another approach for creating MOF-based PDT agents is by fabricating composite materials using PSs and non-intrinsic photodynamic MOFs. The reported structures include PS encapsulation, core-shell structures and surface attachment. This strategy allows for a broader range of PSs beyond porphyrins and their derivatives. Additionally, the selection of MOFs is more diverse, including ZIF-8 (zeolitic imidazolate framework), and UiO-66 (Universitetet i Oslo), MIL-101 (Materials Institute Lavoisier), which are commonly used in therapeutic applications.<sup>27</sup> These modified photodynamic agents are summarized in Table 1. Here, in this section, the therapeutic effect and mechanism of these modified nanocomposites are elaborated, followed by a summary of their modification methods together with their advantages and disadvantages, as detailed in Table 2.

**4.2.1. Loading/encapsulation of PS.** The encapsulation of PSs is a commonly used method to trigger non-intrinsic photodynamic activity in MOFs. In this method, the MOF serves as a container for the PSs, forming a 'ship in a bottle' structure. The PSs that are loaded should have particular functional groups, such as  $-\text{SO}_3\text{H}$  or  $-\text{COOH}$ , or carry an opposite charge to the MOF.<sup>20,80</sup> PS loading/encapsulation can be attained through two strategies, *i.e.*, the *in situ* method (during MOF synthesis) and *ex situ* synthesis (post-synthetic loading).<sup>81</sup> The benefits of encapsulating PSs include preventing their aggregation, inhibiting their contact with oxygen, which hinders the generation of ROS before reaching the tumour site, preventing premature leakage during transport, and enhancing the specificity of PSs to tumors.<sup>68,82</sup>

The use of thermosensitive hydrogels utilizing Zn MOFs is another remarkable strategy to reduce antibiotic use and to improve the antibacterial performance, implementing a safe way for wound healing. Moreover, the drug release mechanism of these gels has the advantage of diffusion, swelling and chemical control compared to other drug administration processes. Ce6@MOF-Gel was comprised of an MOF, with FMOCHis used as the linker and Zn(II) as the metal node together

**Table 2** Summary of different modification methods and their advantages and disadvantages

| Modification methods            | Description   | Advantages  | Disadvantages   |
|---------------------------------|---|---|---|
| Loading/encapsulation of PS     | Encapsulation of the photosensitizers in MOFs with a 'ship in a bottle' architecture, either through <i>in situ</i> or <i>ex situ</i> approach, where <i>in situ</i> generally refers to the method of loading during the MOF synthesis, and <i>ex situ</i> typically implies post-synthetic loading. The method described herein also includes the formation of composite materials by encapsulation or attachment of PSs to MOFs. | <ul style="list-style-type: none"> <li>• Inhibits PS aggregation</li> <li>• Avoids premature ROS generation</li> <li>• Avoids leakage during transport</li> <li>• Increases specificity of PSs to tumors</li> <li>• Possibility of using a wide range of PSs and MOFs</li> <li>• Combination of different therapeutic modalities</li> <li>• Stabilizes and enhances functions.</li> </ul>                                     | <ul style="list-style-type: none"> <li>• Require functional groups on PSs</li> <li>• Limited to MOFs compatible with the PS functional groups</li> <li>• Homogeneity and repeatability problems may occur</li> <li>• Careful management of compatibility between PS and MOF is required.</li> </ul> |
| Surface attachment/modification | PSs are integrated into MOFs by ligand exchange, covalent bonding, or coordination with metal ions, or post-synthetic modification by exchanging ligands or adding functional groups. It offers better positioning of active sites, achieving targeted therapy, and highly promoting the generation of ROS.   | <ul style="list-style-type: none"> <li>• Allows appropriate positioning of the active sites</li> <li>• Facilitates fast assembly and robust attachment</li> <li>• Enhances intracellular ROS generation</li> <li>• Allows broad biomedical application</li> <li>• Enhances generation of ROS in non-photosensitizing MOFs</li> <li>• Allows targeted therapy</li> <li>• Can be theoretically checked and optimized</li> </ul> | <ul style="list-style-type: none"> <li>• May require complicated synthesis procedures</li> <li>• Issues related to the stability of some substrates</li> <li>• Requires extra synthetic steps</li> <li>• Stability issues from modified MOFs.</li> </ul>  |
| Core-shell structure            | Creating core-shell structures through the integration of MOFs with other materials, such as upconversion nanoparticles and gold nanorods, resulting in functionalities that do not exist in a single material.   | <ul style="list-style-type: none"> <li>• Enhances ROS generation through synergistic effects</li> <li>• Provides multifunctional therapeutic effects: for example, PDT, PTT, and CDT</li> <li>• Enhances targeting and accumulation in tumours</li> <li>• Combination of different therapeutic strategies can be done</li> <li>• Can resolve tumor hypoxia and enhance the therapeutic effects.</li> </ul>                    | <ul style="list-style-type: none"> <li>• Potential complexity in synthesis and optimization</li> <li>• Demands accurate control of core-shell interaction</li> <li>• Highly expensive and resource-consuming synthesis</li> <li>• Potential stability and reproducibility issues.</li> </ul>        |





Fig. 8 (a) Preparation and wound healing mechanism of Ce6@MOF-Gel. (b) Excellent biosafety and cell survival rate at 24 h with or without laser radiation. Adapted with permission from ref. 82 Copyright ACS, 2023.

with PS (Ce6) encapsulation. Furthermore, the addition of

hydrogels, which are generally used for the topical administration of drugs.<sup>64</sup> Ce6 is responsible for high-yield ROS generation



under 660 nm irradiation, which is ultimately helpful in wound healing and antibacterial properties.

According to a literature review, Zn MOF has been repeatedly proven to be the best host in drug carrier models. Thus, ZIF-8/Zn MOF subjected to a reformed structure with advanced functionality, particularly forming multimodal active nanocomposites is more effective given that it enhances ROS generation with increasing efficacy in several biomedical applications such as antitumor therapy, antibacterial performance, and wound healing. The detail mechanism together with the survival rate at 24 h is illustrated in Fig. 8(a) and (b), respectively.

Similarly, Zou *et al.* designed biodegradable MOF-coated up-conversion NPs, NaYF<sub>4</sub>:20%Yb,2%Er@Cu/ZIF-8/RB@F127 (UCZRF), for synergistic chemodynamic/photodynamic therapy.<sup>65</sup> The core-shell nanostructure delivered multifunctional facets such as quick degradation of NaYF<sub>4</sub>:20%Yb,2%Er (UCNPs), followed by the release of the loaded PS (RB) and Cu<sup>2+</sup>.

Thus, it facilitated instantaneous light-induced and metal ion-triggered ROS generation. Cu/ZIF-8 in the core-shell could catalyze O<sub>2</sub> to produce ROS and possessed excellent antibacterial activity and low cytotoxicity. The major issue of the inhibition of ROS generation by glutathione (GSH) in TME was resolved by Cu<sup>2+</sup>, given that it uptakes GSH, soon after its release. The efficient uptake of UCZRF and its good biocompatibility were proven by incubated 4T1 and L929 cells under *in vitro* conditions. Furthermore, the intracellular ROS detected

by green fluorescence arose due to the oxidation of 2,7-dichlorodihydrofluorescein (DCFH-DA) to DCF when the 4T1 cells were injected with UCZRF and irradiated with a 980 nm laser light. In addition to its *in vivo* antitumor efficacy, it also showed combined PDT/CDT effects (see Fig. 9).

Cu-MOFs with their unique physicochemical features play a major role in the field of phototherapy given that the redox chemistry of Cu(II) involves the simultaneous effect of glutathione (GSH) oxidation followed by the reaction of reduced Cu(I) with H<sub>2</sub>O<sub>2</sub> to produce ROS.<sup>66</sup> Thus, the therapeutic efficiency increases given that it affects the tumor microenvironment, while also displaying multifunctional behaviour such as anticancer, antibacterial, biosensing, biocatalyst, and wound healing. Besides, the coordination environment of the Cu(II) metal ion directs the ligand in a significant way, and thus the biomaterial formed maintains its porosity and it a potential candidate for cancer theranostics. HDPI (HT@DMSNs-Pt(IV)@ICG) is a type of TME-responsive nanoreactor with high loading efficiency for Pt(IV) prodrug and PS (ICG). HKUST-1 is a widely studied MOF, which has controllable synthesis, together with mesoporous silica nanoparticles as the cornerstone, enabling the efficient loading of PS. DMSNs are used given that they have large pore channels with excellent biocompatibility, and when loaded with Pt(IV) prodrug, their catalytic activities such as catalase (CAT) mimicking, oxidase mimicking and peroxidase (POD) mimicking activities increase. In addition, Pt NPs can also monitor the H<sub>2</sub>O<sub>2</sub>



Fig. 9 TME-responsive UCZRF nanoparticles for enhanced PDT and CDT via GSH depletion and ROS accumulation. Reprinted with permission from ref. 64 Copyright RSC, 2021.



level. ICG is a potential PS, which is mainly used for bioimaging applications due to its absorption in the near IR region and fluorescence emission properties. When irradiated in the range of 800–830 nm light, it exhibits cytotoxic effects in both *in vitro* and *in vivo* environments. The developed nanoreactor is TME responsive with a high release rate of cisplatin in the presence of GSH and  $\text{Cu}^{2+}$  in weakly acidic medium, and its detailed mechanism is illustrated in Fig. 10(b). Moreover, HDPI exhibits excellent stability in neutral medium, but starts degrading at pH 5.5, thus increasing the biosafety and lessening the side effects to normal tissues (Fig. 10a).

Another Cu-MOF-based nanoplatform, Cu-MOF@RCD, with red carbon dot (RCD) doping readily enhanced intracellular ROS generation with the decomposition of  $\text{H}_2\text{O}_2$ . Antitumor immune therapy is implemented with programmed cell death ligand 1 antibody (anti-PD-L1) to facilitate the synergistic effect of photo/chemo dynamic therapy in combination with immune checkpoint blockade therapy.<sup>67</sup> This combination therapy ultimately improves the efficacy given that it improves the host immune system by blocking the negative immune regulatory pathways in TME, particularly depleting GSH and severe hypoxia, and thus enhancing PDT. This also induces antitumor immunity with immunogenic cell death (ICD) in tumor cells, which abolishes primary tumors and inhibits the growth of metastatic tumors. Here, Cu-MOF; HKUST-1 was used as a drug carrier, which is well-known MOF for its adsorption and desorption properties, and also positively charged RCDs were electrostatically adsorbed in the negatively charged mesoporous MOF. In fact, the loading of RCDs did not destroy the crystal form, which shows the robust nature of the modified

Cu-MOF. This study reports that the absorption of RCD increased the ability of the nanocomposite to enhance the PDT/PTT effect in the cancer theranostic platform. Fig. 10(c) illustrates the synergistic effect of the nanocomposite for anti-tumor treatment.

PDT as a promising technique in oncology largely depends on the PS carrier, ROS generation by the PS agent and reaching and deep penetration in the targeted tumor cells, followed by endosomal escape. In this process, the major drawbacks are the detrimental effect of PS on healthy cells and the depletion of ROS generation by antioxidants such as GSH. Thus, nanocomposites are always modified accordingly to minimize the phototoxicity of normal cells. Wang *et al.* developed a new strategy of aggregation-induced emission (AIE) and aggregation-caused quenching (ACQ) of PS and implemented activatable and enhanced image-guided PDT.<sup>68</sup> The well-known MOF-199 (HKUST-1) was employed in the view of its redox-active metal Cu(II), which is prone to oxidizing intracellular GSH. F127 was used with the PS-loaded MOF to prepare NPs. The commercial PS (Ce6) suffers from ACQ, given that it exhibits quenched fluorescence, reducing the generation of  $^1\text{O}_2$ , and therefore a PS (2-(4-(diphenylamino)phenyl)anthraquinone-9,10-dione, TPAAQ) with AIE characteristics was synthesized from triphenylamine and anthraquinone. The comparison of different PSs revealed that TPAAQ is a better AIE-aided PS than the traditional ICG and Ce6. The porous MOF containing the PS isolated it from  $\text{O}_2$ , which quenches ROS production, until the redox active metal ion consumes GSH, followed by the decomposition of the MOF fragments, subsequently triggering the PS in TME to produce intracellular

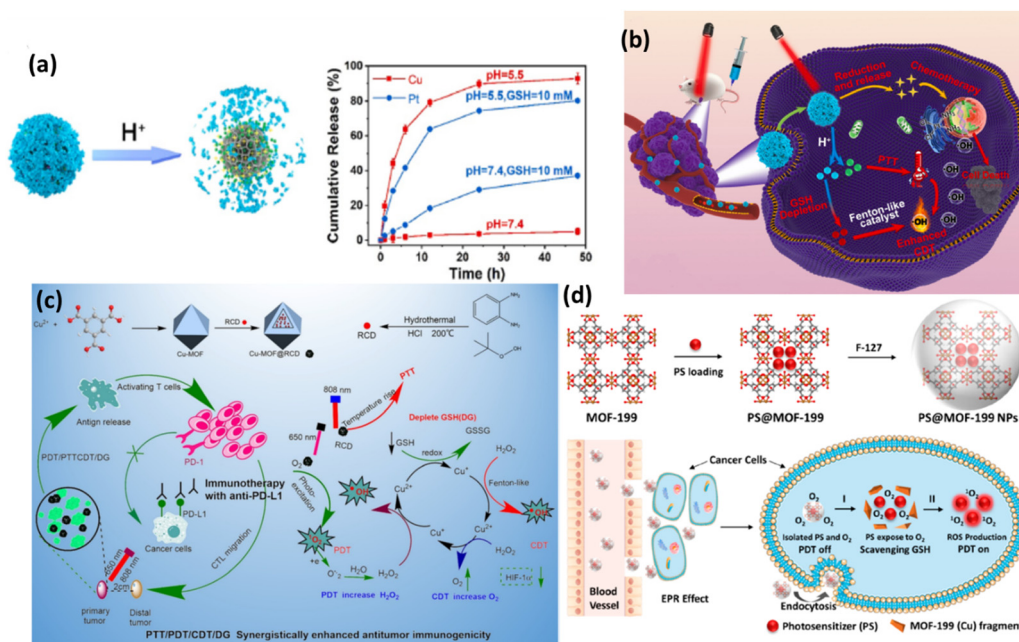


Fig. 10 (a) pH-triggered decomposition of HDPI. (b) Schematic illustration of anticancer mechanism of HDPI. Adapted with permission from ref. 66 Copyright Elsevier, 2022. (c) Preparation and mechanism of action of Cu-MOF@RCD for PDT/CDT/PTTCDT/DG synergistic effect. Reprinted with permission from ref. 67 Copyright RSC, 2023. (d) Synthesis of PS@MOF-199 NPs and PDT on/off mechanism. Adapted with permission from ref. 68 Copyright ELSEVIER, 2022.



$^1\text{O}_2$ . The PDT on and off mechanism are demonstrated in Fig. 10(d).

Bin Liu and coworkers proposed the use of MIL-100 (Fe), an iron(III)-based MOF with large pores, as a carrier for photosensitizers (PSs) to prevent their accumulation in healthy tissues during PDT.<sup>69</sup> Encapsulating PSs in MIL-100 (Fe) limits their photosensitizing capability due to their restricted oxygen access. However, in the presence of excess  $\text{H}_2\text{O}_2$ , often found in tumor sites, MIL-100 (Fe) breaks down, releasing PSs to interact with oxygen and activate PDT. A study used an aggregation-induced emission (AIE) PS, (*E*)-2-(4-(2,2-bis(4-methoxyphenyl)-1-phenylvinyl)styryl)-3-cyano-5,5-dimethylfuran 2(5*H*)ylidene)malononitrile (TPETCF), coated with a non-ionic amphiphilic block copolymer, F127, to improve its water dispersibility for *in vitro* and *in vivo* assays. The PDT effect was demonstrated by cell death induction in 4T1 cells upon exposure to  $\text{H}_2\text{O}_2$  and light irradiation. Tumor-selective activation leverages the higher  $\text{H}_2\text{O}_2$  concentration in tumors, only causing apoptosis in tumor cells. The *in vivo* studies with 4T1 tumor-bearing mice showed that neither TPETCF nor F127-TPETCF@MIL-100 inhibited tumor growth in the dark, whereas both significantly inhibited it upon white light irradiation, with F127-TPETCF@MIL-100 being more effective due to oxygen generation through the reaction between MIL-100 (Fe) and  $\text{H}_2\text{O}_2$ , alleviating tumor hypoxia and boosting the PDT effect. The F127-TPETCF@MIL-100-treated tumors exhibited fewer hypoxic cells, indicating a relieved hypoxic environment. Furthermore, F127-TPETCF@MIL-100 exhibited excellent biocompatibility and negligible *in vivo* toxicity, effectively inhibiting tumor growth upon light irradiation when injected intravenously, highlighting its potential for next-generation therapies.

**4.2.2. Surface attachment/modification.** The active site position in a PDT agent plays a major role given that it significantly inhibits tumor cell growth. Thus, surface attachment/modification in a suitable position can be performed using different methods such as ligand exchange, coordination environment in SBUs,<sup>83</sup> and covalent bonding to pre-functionalized linkers<sup>84,85</sup> and linking groups.<sup>26</sup> Zhao and coworkers assembled ZIF-8 and dopamine (DA) under neutral conditions to produce an extremely robust MOF film for therapeutic use.<sup>70</sup> This fast and facile chelation-induced self-assembly process with an incubation period of 0.5 h overcomes the issue of poor interaction between MOFs and substrates, tedious reaction procedures and low stability of MOF films. The co-deposition of ZIF-8 on substrates prevents the formation of PDA, which is a polymerisation product, and thus often followed in traditional procedures. The chelation reaction between DA and metal ions is attributed to the uniform and firmly attached thin MOF film with the incorporation of ICG, which is a light-responsive nano-agent can be triggered by 10 min NIR light irradiation. The coordination sphere of the metal ion ( $\text{Zn}^{2+}$ ) is dominated by DA chelation, thus disrupting the Zn-imidazole network of ZIF-8, which changes the morphology of the structure. Cross-linkage of ZIF-8/DA reduces the availability of O element, which substantially supports chelation rather than polymerisation. MOF films, particularly employed

as antibacterial surfaces, have a wide range of biomedical applications such as wound dressings, masks, and protective suits. Intracellular ROS generation was detected by DPBV, while the *in vitro* antibacterial tests on *S. aureus* and *E. coli* were successful, as shown in Fig. 11(a) and (b).

Nano-scale composites in the form of nanozymes, films and hydrogels deliver enhanced PDT with various imaging functions. ZIF-8 is the most widely used MOF due to its simple synthetic strategy with advanced properties particularly in biomedical applications, given that it acts as a brilliant host for enzymes, proteins, drugs, *etc.* Yang *et al.* reported the preparation of a nanozyme, which is a platinum-carbon integrated composite, ultimately enhancing PDT and accelerating ROS generation in the near IR region.<sup>71</sup> Consequently, the cytotoxic agent  $^1\text{O}_2$  generated from the nanozyme is trapped by ABDA, forming endoperoxide. The strong catalase-type activity results in more dead cells and removes tumor hypoxia, thus also overcoming the limitation of traditional photosensitizers with 90% tumor inhibition rate. The synergistic PTT and PDT antitumor effect on a CT26 subcutaneous tumor model was also investigated. The relative cell viability in both normoxic and hypoxic conditions showed that the *in vitro* PDT/PTT efficacy depends on the integration of Pt-carbon and presence of oxygen. The removal of tumor hypoxia *in vivo* was also tested in CT26 cells, showing intense oxyhaemoglobin photoacoustic signals.

Pang and coworkers successfully synthesized a mixed-ligand MOF by exchanging the functional ligand 1,3,6,8-tetrakis(*p*-benzoic acid)pyrene ( $\text{H}_4\text{TBAPy}$ ) in NU-1000 by TCPP, porphyrinic ligand *via* a post-synthetic ligand exchange method. To stabilise the MOF and make it useful in biomedical applications, the mixed nanoscale MOF was further modified with PEG and folic acid (FA) to form NT@PEG@FA.<sup>55</sup> Interestingly, after modification, TCPP was not absorbed in the MOF, rather it coordinated to the  $\text{Zr}_6$  cluster, as shown in Fig. 11(c), whereas TPP was not coordinated. Under laser irradiation, there was a significant increase in ROS generation due to the TCPP in the mixed MOF in comparison to NU-1000. The PDT effect was evaluated using ICG as the indicator. The substitution effect was also further evaluated theoretically. This example opens the path for non-PDT@MOF materials exhibiting none or low photosensitizing properties to be functionalised *via* post-synthetic modification to induce ROS generation, thus enhancing their antitumor efficacy.

**4.2.3. Core-shell structure.** The study by Song *et al.* presented  $\beta\text{-NaYF}_4\text{:Yb,Tm,Gd@MIL-100(Fe)}$ , a new near-infrared (NIR) light-responsive nanomaterial developed for antibacterial PDT. This material was synthesized using the solvothermal and layer-by-layer self-assembly methods and featured a core-shell structure with up-conversion nanorods (UCNRs) and MIL-100(Fe) shell. It exhibited strong fluorescence and enhanced antibacterial properties.<sup>73</sup> Under 980 nm laser excitation, UCNR@MIL-100(Fe) produced ROS, triggering a photo-Fenton reaction that is effective against both Gram-positive and Gram-negative bacteria. Its antibacterial action was based on ROS generation, as indicated by the reduced absorption of DPBF at 410 nm under 980 nm light, showing the





Fig. 11 (a) Preparation process ZIF-8/DA-0.5 and ZIF-8/DA-0.5/ICG composite. (b) Deposition of ZIF-8 on substrate with DA. Adapted with permission from ref. 70 Copyright RSC, 2022. (c) Preparation of mixed MOF NT by post-synthetic modification of NU-1000 for photodynamic therapy. Reprinted with permission from ref. 55 Copyright RSC, 2023.

ability of this nanomaterial to produce ROS with or without light. The cytotoxicity tests confirmed the low toxicity and high biocompatibility of the UCNR@MIL-100(Fe) composites. The antibacterial tests against *E. coli* and *S. aureus* revealed that although its individual components had low toxicity, combining  $1 \text{ mg mL}^{-1}$  UCNR@MIL-100(Fe) with  $100 \text{ mM H}_2\text{O}_2$  significantly decreased bacterial colonies by approximately 37% and 39%, respectively, due to the hydroxyl radicals generated by the Fenton reaction. Exposing this combination to  $980 \text{ nm}$  light for  $15 \text{ min}$  without  $\text{H}_2\text{O}_2$  led to a 60% reduction in bacterial colonies, whereas the same exposure in the presence of  $\text{H}_2\text{O}_2$  inactivated 99.6% of *E. coli* and 99.2% of *S. aureus*, showcasing the strong antibacterial effect of photodynamic therapy and the Fenton reaction. Extending the irradiation time to  $18 \text{ min}$  nearly eradicated all the bacteria, underscoring the potential of UCNR@MIL-100(Fe) for treating bacterial infections.

A novel MOF-coated upconversion nanoconstruct (UCTSCF) for synergistic photo-chemodynamic therapy (PCT) and oxygen-elevated PDT in cancer treatment was introduced by Chu *et al.*, addressing challenges such as hypoxic tumor environment and stringent activation conditions.<sup>74</sup> UCTSCF was comprised of an  $808 \text{ nm}$ -driven upconversion nanoparticle (UC) core, chlorin e6 (Ce6) photosensitizer, oxygen-carrying compound (TFS) co-doped mesoporous silicon layer, and Cu-doped MIL-100(Fe) MOF coating (Fig. 12a). This design provides intense blue light for PCT and facilitates oxygen-elevated  $^1\text{O}_2$  production for enhanced PDT. The cellular uptake studies in MCF-7 cells showed the efficient internalization of UCTSCF, as indicated by the increase in Ce6 fluorescence. The biocompatibility tests with L929 mouse fibroblasts demonstrated no significant

toxicity at high UCTSCF concentrations and no adverse effects from  $808 \text{ nm}$  laser irradiation. The *in vitro* assays revealed that UCTSCF exhibited low dark toxicity but significantly reduced MCF-7 cell viability under  $808$  or  $671 \text{ nm}$  laser irradiation, highlighting its potential for combined PCT and PDT. The synergistic therapeutic effect was further confirmed by the increase in ROS generation in the treated MCF-7 cells, which was observed through DCF fluorescence, and enhanced anti-tumor efficacy, reducing the cell viability to approximately 20%. The calcein/PI cell viability/cytotoxicity assay corroborated the synergistic cytotoxicity of UCTSCF under combined laser irradiation.

Cai and team developed core-shell hybrids with gold nanorods (AuNRs) as the core for PTT and an MOF shell with a porphyrin ligand for PDT through the layer-by-layer method, enabling tunable therapeutic effects.<sup>60</sup> The AuNRs exhibit strong absorbance at  $650 \text{ nm}$ , converting light into heat, while the porphyrin in the MOF shell generates singlet oxygen ( $^1\text{O}_2$ ) under light conditions, a key reactive species in PDT. This study demonstrated that the Au@MOF hybrids effectively produced heat and singlet oxygen, leading to synergistic therapeutic effects. To address the challenge of the hypoxic tumor environment, which limits singlet oxygen production, the MOF structure incorporates a metal node,  $\text{Fe}_3\text{O}(\text{OAc})_6(\text{H}_2\text{O})^{3+}$ , which catalyzes the decomposition of hydrogen peroxide ( $\text{H}_2\text{O}_2$ ) into oxygen, enhancing the PDT effect. The Au@MOF hybrids exhibited good biocompatibility and no significant toxicity in the cellular and animal experiments. Surface modification with folic acid enhanced their targeting of cancer cells with overexpressed folate receptors, leading to the enhanced accumulation of the





Fig. 12 (a) Process for the preparation of UCTSCF and light-triggered combo therapy PDT/PTT. Adapted with permission from ref. 74 Copyright RSC, 2022. (b) Working mechanism of Au@MOF core-shell hybrids. Reprinted with permission from ref. 60 Copyright RSC, 2023.

hybrids at the tumor site and improved inhibitory effect on tumor growth. The therapeutic efficacy was assessed *in vitro* with cervical cancer cells (CaSki) and *in vivo* using a CaSki tumor-bearing mouse model, showing effective cancer cell killing and tumor growth inhibition under light irradiation without major organ damage, as shown in Fig. 12(b). These results demonstrate the potential of the Au@MOF hybrids as a multifunctional platform for cancer therapy.

#### 4.3. Stimulus-responsive MOFs in PDT

MOFs with stimulus-responsive groups possess advanced properties compared to conventional modalities, making their use another successful approach in the development of PDT. Exogenous stimuli when activated by temperature/pressure/light/magnetic/ions and endogenous stimuli in response to pH/enzyme/redox in the tumour microenvironment have been reported, executing the physical or chemical transformation of drug-loaded stimuli responsive MOF-based systems.<sup>86</sup> In this process, both single or multiple stimulus-responsive MOFs are designed to provide controllable drug delivery in various cancer treatments and other biomedical applications.

pH-activated MOFs are the most widely used stimuli-responsive MOFs, given that they are affected by any chemical reactions such as protonation and degradation of associated compounds in the tumor microenvironment. The nanotheranostic system Zr-MOF@PPa/AF@PEG was designed and developed by Wang *et al.* It was stable at pH 7.4, and most importantly under slightly acidic condition, it activated the PS, pyropheophorbide-a

(PPa) and consumed oxygen with the smooth release of the hypoxic-sensitive drug AF (6-amino flavone), thus removing the hypoxic condition, which is a general challenge encountered in PDT anticancer treatments<sup>76</sup> (Fig. 13a). Another dual-responsive triple synergistic Fe-MOF for anti-tumor treatment was reported by Chen *et al.*, PCN-DOX@PDA system. It was developed considering the weak acidic tumour microenvironment to facilitate PDT and thermal stimulation generated by NIR radiation responsible for PTT together with magnetic resonance imaging, contributing a triple synergistic effect for cancer therapy, as discussed in Section 4.1.1.<sup>57</sup>

Similarly, enzyme-responsive nano-platforms enable enzyme-triggered, controlled drug delivery, antibacterial PDT and other biomedical applications. Kun Na and co-workers reported lipase-sensitive singlet oxygen production, which ultimately enhanced PDT to cure *P. acnes*-caused skin inflammation, as shown in Fig. 13(b). The controlled drug delivery of erythromycin and Pheo A (PS), due to the selective cleavage of the ester bonds in DPPC (1,2-dipalmitoyl-*sn*-phosphatidylcholine) by *P. acnes* lipase resulted in an innovative method to combat bacteria-induced skin disorders. Thus, the well-known erythromycin is responsible for antimicrobial activity against infection, whereas laser irradiation induces the combination of *P. acnes* growth and inflammation containing *P. acnes*, producing singlet oxygen and facilitating antimicrobial PDT.<sup>77</sup>

Factors such as pH, ROS, temperature, and light can be employed successfully to trigger the release of anticancer drugs; however, the controlled release of therapeutic agents and



Fig. 13 (a) Synergistic anti-tumor mechanism of photodynamic therapy (PDT) and chemotherapy (CT). Adapted with permission from ref. 76 Copyright Elsevier, 2021. (b) Schematic representation of the lipase-sensitive singlet oxygen production and combination mechanism of antibacterial and singlet oxygen. Adapted with permission from ref. 77 Copyright Elsevier, 2017.



reduction in off-target effects can effectively be achieved using redox-responsive agents in PDT. Redox-responsive MOFs can be designed for controlled drug release in response to the specific redox environment found in tumour cells, enabling effective PDT. Furthermore, these MOFs can be modified with targeting ligands for preferential accumulation in tumour tissues. Upon entering the tumor environment, the redox-responsive components of the MOF undergo redox reaction (oxidation/reduction), triggering the release of the therapeutic agents/photosensitizer. Presently, selenium-containing polymers have attracted significant attention owing to their exceptional redox-responsive capabilities and potential role in cancer prevention. In this regard, Luo *et al.* also developed a light-induced redox responsive core-shell MOF using a photosensitive porphyrin Zr-MOF as the core and Se-substituted polymer as the shell *via* the emulsion approach (Fig. 14a) for combinatorial photodynamic and chemotherapy. The redox-sensitive di-(1-hydroxylundecyl) selenide (DH-Se), biocompatible poly(propylene glycol) (PPG) and poly(ethylene glycol) (PEG) were polymerized randomly to generate poly(DH-Se/PEG/PPG urethane), which was further used to coat ROS-producing PCN-224, leading to the formation of poly(DH-Se/PEG/PPG urethane)@MOF shell-core NPs. Interestingly, the NPs when loaded with doxorubicin (DOX), a chemotherapeutic agent, exhibited rapid and controllable releasing ability, facilitating combined application of chemotherapy and photodynamic therapy upon laser illumination. The laser-driven ROS generation induced the cleavage of the poly(DH-Se/PEG/PPG urethane) polymer chain, resulting in the release of DOX. As demonstrated in Fig. 14(b), the stimulus-sensitive drug release ability of poly(DH-Se/PEG/PPG urethane)@MOF was evaluated by releasing DOX as a model drug in phosphate buffer saline (PBS) *in vitro* after the confirmation of the efficacy of this material for light-induced structural breaking

and ROS generation. The drug-loaded DOX/poly(DH-Se/PEG/PPG urethane)@MOF nanocomposite was produced by further sonicating DOX@poly(DH-Se/PEG/PPG urethane) micelles and PCN-224 MOF. This was possible due to the hydrophobic section of the PPG block, which allowed poly(DH-Se/PEG/PPG urethane) to form micelles, trapping DOX. Less than 20% of the DOX from the DOX/poly(DH-Se/PEG/PPG urethane)@MOF nanocomposite was released *in vitro* in less than 48 h; however, this release process was greatly accelerated by laser illumination. This was most likely the outcome of the ROS produced by the porphyrin PCN-224 MOF-induced breakage of the selenium-containing polymer chain in response to light stimulation.

Increased levels of oxidants, particularly ROS indicate an inflammatory milieu and are linked to several inflammatory disorders, including neurological diseases, diabetes, cancer, and atherosclerosis. Accordingly, the delivery of anti-inflammatory medications *via* oxidation-responsive smart devices is a sensible approach. In addition to lowering the necessary treatment dose and minimizing adverse effects, this strategy guarantees the targeted release of medication at the site of inflammation. Oxidation-responsive poly-MOF nanoparticles (NPs) were created by Zhou *et al.* to be used in combinatorial increased stimulator of interferon gene (STING) activation in conjunction with photodynamic immunotherapy (PDIT). After the PMOF NPs were synthesized with poly(ethylene glycol) (PEG) shells, the STING agonist (SR-717) was loaded into the PMOF to create SR@PMOF NPs.<sup>79</sup> These NPs exhibited excellent stability in physiological conditions because of the incorporation of polymer ligands and could efficiently generate ROS upon exposure to light irradiation, which breaks the thioketal bonds and releases SR-717 quickly. To improve the stability for drug delivery, MOF NPs with PEG shells were prepared using the block copolymer PEG-*b*-PABDA.



Fig. 14 (a) Illustration of synthesis of DH-Se/PEG/PPG urethane. (b) Mechanism of structure breaking after light illumination and release of the anticancer drug DOX. Adapted with permission from ref. 78 Copyright Wiley-VCH, 2019. (c) Synthesis and mechanism of SR@PMOF, ROS generation and enhanced STING activation at tumor site. Adapted with permission from ref. 79 Copyright ACS, 2023.



In addition, thioketal bonds were added to the PMOF to release SR-717, which is responsive to ROS. The porous and crystalline structure of PMOF NPs, where the TCPP photosensitizers were separated to prevent self-quenching, allowed the TCPP photosensitizers to efficiently create ROS after intravenous administration and accumulation in the tumor tissues. The  $^1\text{O}_2$  generated by SR@ PMOF has the potential to eliminate associated tumor cells and break down thioketal linkages, resulting in the breakdown of MOF particles and the liberation of SR-717 for use in combination with photodynamic and immune therapy. The tumor-associated antigens that have been released, DNA fragments, and SR-717 can effectively activate the STING pathway to support dendritic cell maturation. Subsequently, these cells migrate to the lymph nodes to polarize CD8<sup>+</sup>T lymphocytes. Improved levels of CD8<sup>+</sup>T cells were found in the lymph nodes and the main tumors. By PDT-induced reversal of the immunosuppressive tumor microenvironment and oxidation-triggered release of STING agonists for increased antitumor immunity, the SR@PMOF NPs exhibited a synergistic enhancement in STING activation. Fig. 14(c) shows the entire experimental process from synthesis to production of ROS.

## 5. Conclusion and future perspectives

Over the last four decades, significant advancements have been extensively explored in PDT given that it is one of the most promising approaches to treat various oncological (cancer therapy) and non-oncological disorders (wound healing and antimicrobial therapy). However, despite these advancements, PDT is still limited as a primary treatment option, owing to the limitations associated with traditional PSs. To date, although numerous PDT agents have entered clinical trials or have been clinically approved, they are not suitable for consideration as first-line treatments. Recent progress in nanotechnology offers exciting prospects for designing PDT systems. These advancements present versatile opportunities to address the current challenges in PDT, such as designing bioactive MOFs that can serve as effective PS agents.

This review highlighted the recent progress in using MOF-based photosensitizers (PS) for photodynamic cancer therapy, antibacterial therapy, and wound healing. The evolution of PS generations has demonstrated that nanotechnology offers a promising approach to improve PS delivery, enhancing their distribution in the body and pharmacokinetics, and thereby maximizing the PDT efficiency, while minimizing side effects. Despite the challenges encountered such as PS aggregation in nano-carriers and the biocompatibility and biodegradability of PSs when combined with inorganic nanoparticles, recent developments in MOF nanocarriers with integrated PS molecules show promise in overcoming these hurdles. These new nano-photosensitizers represent a significant advancement in finding ideal PSs. By integrating PS agents and other targeted therapeutic agents in MOFs, together with diverse modifications, PDT treatment can be improved by overcoming the constraints of earlier generations of PS. In the evolution of the advancement in therapeutic techniques, stimuli-responsive MOFs, in particular,

play another major role in theranostic platforms exclusively, given that they depend on exogenous or endogenous stimuli-triggered mechanisms for smooth and effective PDT with various biomedical applications. These incorporated agents and modified methods establish a versatile platform for investigating synergy and combination therapy, resulting in clinical advantages for treating metastatic cancer and other complex cancer cases. However, to achieve benchmark efficacy, transitioning from the laboratory to clinical application, the following points need to be considered:

(1) *In vitro* and *in vivo* research indicates that MOFs have low toxicity, but it is important to assess their cytotoxicity levels accurately. Furthermore, *in vivo* studies examining how these materials are absorbed, distributed, metabolized, and excreted will reveal if there is any accumulation of toxic metals. These assessments are crucial for establishing safe therapeutic dosages for *in vivo* trials and enabling the translation of MOFs into clinical research. Also, the stimuli-responsive properties of NMOFs should be considered, especially concerning the tumor microenvironment. This approach can result in versatile platforms that accurately target and release drugs at the tumor site, improving the therapy efficacy.

(2) There is ample opportunity for improvement in terms of shrinking the size of the structure, enhancing the stability of PS loading, optimizing parameters for PDT, and ultimately enhancing the PDT effectiveness. Collaboration between scientists, academics, engineers, clinicians, and industrial innovators is crucial in this multidisciplinary field to exchange ideas and address challenges, with the goal of advancing PDT for oncological diagnosis and treatment. The future of PDT depends on creating singular, adaptable, and effective nanoparticles that can be used for both bioimaging and PDT.

## Data availability

Data will be made available on request.

## Conflicts of interest

There are no conflicts to declare.

## Acknowledgements

All the authors are grateful to Siksha O' Anusandhan (Deemed to be) University for providing funding and lab facilities. One of the author, Newmoon Priyadarshini is grateful to CSIR for awarding SRF.

## References

- 1 D. W. Felsher, *Nat. Rev. Cancer*, 2003, **3**, 375–380.
- 2 G. Lan, K. Ni and W. Lin, *Coord. Chem. Rev.*, 2019, **379**, 65–81.
- 3 K. K. Ng and G. Zheng, *Chem. Rev.*, 2015, **115**, 11012–11042.



- 4 X. Li, S. Kolemen, J. Yoon and E. U. Akkaya, *Adv. Funct. Mater.*, 2017, **27**, 1604053.
- 5 A. G. Niculescu and A. M. Grumezescu, *Appl. Sci.*, 2021, **11**, 3626.
- 6 M. R. Hamblin, *Photochem. Photobiol. Sci.*, 2018, **17**, 1515–1533.
- 7 M. D. Daniell and J. S. Hill, *Aust. N. Z. J. Surg.*, 1991, **61**, 340–348.
- 8 S. Kwiatkowski, B. Knap, D. Przystupski, J. Saczko, E. Kędzierska, K. Knap-Czop, J. Kotlińska, O. Michel, K. Kotowski and J. Kulbacka, *Biomed. Pharmacother.*, 2018, **106**, 1098–1107.
- 9 J. F. Algorri, M. Ochoa, P. Roldán-Varona, L. Rodríguez-Cobo and J. M. López-Higuera, *Cancers*, 2021, **13**, 4447.
- 10 I. S. Turan, D. Yildiz, A. Turksoy, G. Gunaydin and E. U. Akkaya, *Angew. Chem.*, 2016, **128**, 2925–2928.
- 11 S. S. Lucky, K. C. Soo and Y. Zhang, *Chem. Rev.*, 2015, **115**, 1990–2042.
- 12 N. Priyadarshini, K. Kumar Das, S. Mansingh and K. Parida, *Results Chem.*, 2022, **4**, 100450.
- 13 S. Mansingh, S. Subudhi, S. Sultana, G. Swain and K. Parida, *ACS Appl. Nano Mater.*, 2021, **4**, 9635–9652.
- 14 S. P. Tripathy, S. Subudhi and K. Parida, *Coord. Chem. Rev.*, 2021, **434**, 213786.
- 15 P. Behera, S. Subudhi, S. P. Tripathy and K. Parida, *Coord. Chem. Rev.*, 2022, **456**, 214392.
- 16 J. Panda, S. P. Tripathy, S. Dash, A. Ray, P. Behera, S. Subudhi and K. Parida, *Nanoscale*, 2023, **15**, 7640–7675.
- 17 P. Priyadarshini and K. Parida, *J. Energy Storage*, 2024, **87**, 111379.
- 18 Q. Guan, Y. A. Li, W. Y. Li and Y. Bin Dong, *Chem. – Asian J.*, 2018, **13**, 3122–3149.
- 19 G. Gunaydin, M. E. Gedik and S. Ayan, *Front. Chem.*, 2021, **9**, 691697.
- 20 Q. Zheng, X. Liu, Y. Zheng, K. W. K. Yeung, Z. Cui, Y. Liang, Z. Li, S. Zhu, X. Wang and S. Wu, *Chem. Soc. Rev.*, 2021, **50**, 5086–5125.
- 21 R. Masoudifar, N. Pouyanfar, D. Liu, M. Ahmadi, B. Landi, M. Akbari, S. Moayeri-Jolandan, F. Ghorbani-Bidkorpeh, E. Asadian and M. A. Shahbazi, *Appl. Mater. Today*, 2022, **29**, 101646.
- 22 M. R. Saeb, N. Rabiee, M. Mozafari, F. Verpoort, L. G. Voskressensky and R. Luque, *Materials*, 2021, **14**, 7277.
- 23 P. D. Fernandes, F. D. Magalhães, R. F. Pereira and A. M. Pinto, *Polymers*, 2023, **15**, 1490.
- 24 Y. Zhao, X. Jiang, X. Liu, X. Liu, Z. Liu and X. Liu, *Front. Bioeng. Biotechnol.*, 2022, **10**, 1031986.
- 25 X. Cai, Y. Zhao, L. Wang, M. Hu, Z. Wu, L. Liu, W. Zhu and R. Pei, *J. Mater. Chem. B*, 2021, **9**, 6646–6657.
- 26 J. Yang and Y. W. Yang, *VIEW*, 2020, **1**, e20.
- 27 D. Zhao, W. Zhang, S. Yu, S. L. Xia, Y. N. Liu and G. J. Yang, *J. Nanobiotechnol.*, 2022, **20**, 421.
- 28 X. Chen, S. M. Argandona, F. Melle, N. Rampal and D. Fairen-Jimenez, *Chem*, 2024, **10**, 504–543.
- 29 S. R. Alves, I. R. Calori and A. C. Tedesco, *Mater. Sci. Eng., C*, 2021, **131**, 112514.
- 30 N. Alvarez and A. Sevilla, *Int. J. Mol. Sci.*, 2024, **25**, 1023.
- 31 J. M. Dąbrowski and L. G. Arnaut, *Photochem. Photobiol. Sci.*, 2015, **14**, 1765–1780.
- 32 S. Kwiatkowski, B. Knap, D. Przystupski, J. Saczko, E. Kędzierska, K. Knap-Czop, J. Kotlińska, O. Michel, K. Kotowski and J. Kulbacka, *Biomed. Pharmacother.*, 2018, **106**, 1098–1107.
- 33 Z. Bao, K. Li, P. Hou, R. Xiao, Y. Yuan and Z. Sun, *Mater. Chem. Front.*, 2021, **5**, 1632–1654.
- 34 A. P. Castano, P. Mroz and M. R. Hamblin, *Nat. Rev. Cancer*, 2006, **6**, 535–545.
- 35 R. Ackroyd, C. Kelty, N. Brown and M. Reed, *Photochem. Photobiol.*, 2001, **74**, 656–669.
- 36 T. J. Dougherty, C. J. Gomer, B. W. Henderson, G. Jori, D. Kessel, M. Korbelik, J. Moan and Q. Peng, *J. Natl. Cancer Inst.*, 1998, **90**, 889–905.
- 37 J. Zhang, C. Jiang, J. P. Figueiró Longo, R. B. Azevedo, H. Zhang and L. A. Muehlmann, *Acta Pharm. Sin. B*, 2018, **8**, 137–146.
- 38 R. V. Huis in 't Veld, J. Heuts, S. Ma, L. J. Cruz, F. A. Ossendorp and M. J. Jager, *Pharmaceutics*, 2023, **15**, 330.
- 39 P. de Silva, M. A. Saad, H. C. Thomsen, S. Bano, S. Ashraf and T. Hasan, *J. Porphyrins Phthalocyanines*, 2020, **24**, 1320–1360.
- 40 L. Ming, K. Cheng, Y. Chen, R. Yang and D. Chen, *Cancer Med.*, 2021, **10**, 257–268.
- 41 J. H. Correia, J. A. Rodrigues, S. Pimenta, T. Dong and Z. Yang, *Pharmaceutics*, 2021, **13**, 1332.
- 42 J. Kou, D. Dou and L. Yang, *Oncotarget*, 2017, **8**, 81591–81603.
- 43 E. Foresto, P. Gilardi, L. E. Ibarra and I. S. Cogno, *Phytomed. Plus*, 2021, **1**, 100044.
- 44 T. Hsia, J. L. Small, A. Yekula, S. M. Batool, A. K. Escobedo, E. Ekanayake, G. D. You, H. Lee, B. S. Carter and L. Bajaj, *Cancers*, 2023, **15**, 3918.
- 45 R. R. Allison, G. H. Downie, R. Cuenca, X. H. Hu, C. J. H. Childs and C. H. Sibata, *Photodiagn. Photodyn. Ther.*, 2004, **1**, 27–42.
- 46 A. B. Ormond and H. S. Freeman, *Materials*, 2013, **6**, 817–840.
- 47 L. B. Josefsen and R. W. Boyle, *Met. Based Drugs*, 2008, 276109.
- 48 H. Yu, B. Chen, H. Huang, Z. He, J. Sun, G. Wang, X. Gu and B. Z. Tang, *Biosensors*, 2022, **12**.
- 49 P. Agostinis, K. Berg, K. A. Cengel, T. H. Foster, A. W. Girotti, S. O. Gollnick, S. M. Hahn, M. R. Hamblin, A. Juzeniene, D. Kessel, M. Korbelik, J. Moan, P. Mroz, D. Nowis, J. Piette, B. C. Wilson and J. Golab, *CA-Cancer J. Clin.*, 2011, **61**, 250–281.
- 50 W. Park, S. Cho, J. Han, H. Shin, K. Na, B. Lee and D. H. Kim, *Biomater. Sci.*, 2018, **6**, 79–90.
- 51 Z. Fu, S. Li, S. Han, C. Shi and Y. Zhang, *Signal Transduction Targeted Ther.*, 2022, **7**, 93.
- 52 I. S. Mfouo-Tynga, L. D. Dias, N. M. Inada and C. Kurachi, *Photodiagn. Photodyn. Ther.*, 2021, **34**, 102091.



- 53 A. Eras, D. Castillo, M. Suárez, N. S. Vispo, F. Albericio and H. Rodriguez, *Front. Chem.*, 2022, **10**, 889083.
- 54 G. Wei, X. Lian, X. Qin, Y. Zhao, L. Cai, Q. Chen, J. J. Zou and J. Tian, *Mater. Des.*, 2022, 111302.
- 55 X. Zhao, L. Chang, Y. Hu, S. Xu, Z. Liang, X. Ren, X. Mei and Z. Chen, *ACS Appl. Mater. Interfaces*, 2022, **14**, 18194–18208.
- 56 K. Zhang, X. Meng, Y. Cao, Z. Yang, H. Dong, Y. Zhang, H. Lu, Z. Shi and X. Zhang, *Adv. Funct. Mater.*, 2018, **28**, 1804634.
- 57 Z. Chen, Y. Sun, J. Wang, X. Zhou, X. Kong, J. Meng and X. Zhang, *ACS Nano*, 2023, **17**, 9003–9013.
- 58 G. Lan, K. Ni, S. S. Veroneau, X. Feng, G. T. Nash, T. Luo, Z. Xu and W. Lin, *J. Am. Chem. Soc.*, 2019, **141**, 4204–4208.
- 59 X. Zheng, L. Wang, Y. Guan, Q. Pei, J. Jiang and Z. Xie, *Biomaterials*, 2020, **235**, 119792.
- 60 X. Cai, Z. Xie, B. Ding, S. Shao, S. Liang, M. Pang and J. Lin, *Adv. Sci.*, 2019, **6**, 1900848.
- 61 S. Y. Liu, Y. Xu, H. Yang, L. Liu, M. Zhao, W. Yin, Y. T. Xu, Y. Huang, C. Tan, Z. Dai, H. Zhang, J. P. Zhang and X. M. Chen, *Adv. Mater.*, 2021, 2100849.
- 62 W. Wang, L. Wang, Z. Li and Z. Xie, *Chem. Commun.*, 2016, **52**, 5402–5405.
- 63 J. Park, Q. Jiang, D. Feng and H. Zhou, *Angew. Chem.*, 2016, **128**, 7304–7309.
- 64 W. Zhang, B. Wang, G. Xiang, T. Jiang and X. Zhao, *ACS Appl. Mater. Interfaces*, 2023, **15**, 22830–22842.
- 65 M. Zou, Y. Zhao, B. Ding, F. Jiang, Y. Chen, P. Ma and J. Lin, *Inorg. Chem. Front.*, 2021, **8**, 2624–2633.
- 66 Y. Bian, B. Liu, S. Liang, B. Ding, Y. Zhao, F. Jiang, Z. Cheng, A. A. A. Kheraif, P. Ma and J. Lin, *Chem. Eng. J.*, 2022, **435**, 135046.
- 67 Z. Su, H. Xu, Y. Zhang, H. Zhang, H. Zhang, Y. Bao, X. Wu, R. Yan, G. Tan, Z. Wang and Y. Jin, *J. Mater. Chem. B*, 2023, **11**, 4211–4226.
- 68 Y. Wang, W. Wu, J. Liu, P. N. Manghnani, F. Hu, D. Ma, C. Teh, B. Wang and B. Liu, *ACS Nano*, 2019, **13**, 6879–6890.
- 69 F. Hu, D. Mao, Kenry, Y. Wang, W. Wu, D. Zhao, D. Kong and B. Liu, *Adv. Funct. Mater.*, 2018, **28**, 1707519.
- 70 J. Gao, L. Hao, R. Jiang, Z. Liu, L. Tian, J. Zhao, W. Ming and L. Ren, *Green Chem.*, 2022, **24**, 5930–5940.
- 71 Y. Yang, D. Zhu, Y. Liu, B. Jiang, W. Jiang, X. Yan and K. Fan, *Nanoscale*, 2020, **12**, 13548–13557.
- 72 X. Zhao, Z. Zhang, X. Cai, B. Ding, C. Sun, G. Liu, C. Hu, S. Shao and M. Pang, *ACS Appl. Mater. Interfaces*, 2019, **11**, 7884–7892.
- 73 J. Song, L. Sun, H. Geng, W. Tan, D. Zhen and Q. Cai, *New J. Chem.*, 2022, **46**, 4806–4813.
- 74 H. Chu, Y. Li, C. Wang, J. W. Shen and Y. Wei, *Dalton Trans.*, 2022, **51**, 16336–16343.
- 75 X. Cai, Y. Zhao, L. Wang, M. Hu, Z. Wu, L. Liu, W. Zhu and R. Pei, *J. Mater. Chem. B*, 2021, **9**, 6646–6657.
- 76 X. Wang, Z. Wang, W. Ma, X. Wu, W. Fang, C. Guo and Y. Jin, *J. Photochem. Photobiol., B*, 2021, **222**, 112274.
- 77 S. Jeong, J. Lee, B. N. Im, H. Park and K. Na, *Biomaterials*, 2017, **141**, 243–250.
- 78 Z. Luo, L. Jiang, S. Yang, Z. Li, W. M. W. Soh, L. Zheng, X. J. Loh and Y. L. Wu, *Adv. Healthcare Mater.*, 2019, **8**, 1900406.
- 79 Q. Zhou, D. Dutta, Y. Cao and Z. Ge, *ACS Nano*, 2023, **17**, 9374–9387.
- 80 H. Zhang, Q. Li, R. Liu, X. Zhang, Z. Li and Y. Luan, *Adv. Funct. Mater.*, 2018, **28**, 1802830.
- 81 Y. Wang, J. Yan, N. Wen, H. Xiong, S. Cai, Q. He, Y. Hu, D. Peng, Z. Liu and Y. Liu, *Biomaterials*, 2020, **230**, 119619.
- 82 F. Nian, Y. Huang, M. Song, J. J. Chen and J. Xue, *J. Mater. Chem. B*, 2017, **5**, 6227–6232.
- 83 B. Liu, M. Ma, D. Zacher, A. Bétard, K. Yusenko, N. Metzler-Nolte, C. Wöll and R. A. Fischer, *J. Am. Chem. Soc.*, 2011, **133**, 1734–1737.
- 84 A. Zimpel, T. Preiß, R. Röder, H. Engelke, M. Ingrisich, M. Peller, J. O. Rädler, E. Wagner, T. Bein and U. Lächelt, *Chem. Mater.*, 2016, **28**, 3318–3326.
- 85 W. H. Yin, Y. Y. Xiong, H. Q. Wu, Y. Tao, L. X. Yang, J. Q. Li, X. L. Tong and F. Luo, *Inorg. Chem.*, 2018, **57**, 8722–8725.
- 86 W. Cai, J. Wang, C. Chu, W. Chen, C. Wu and G. Liu, *Adv. Sci.*, 2019, **6**, 1801526.

